AGU PUBLICATIONS

Geophysical Research Letters

RESEARCH LETTER

10.1002/2016GL070083

Key Points:

- Wide fault zones produce a chaotic and dispersive wavefront in the upper mantle at the outer rise
- The presence of hydrated fault zones explains observed slowing in upper mantle velocities
- Hydrated fault zones require far less water than uniformly serpentinized upper mantle to produce similar degrees of wavefront slowing

Correspondence to:
N. C. Miller,
ncmiller@usgs.gov

Citation:
Miller, N. C., and D. Lizarralde (2016), Finite-frequency wave propagation through outer rise fault zones and seismic measurements of upper mantle hydration, *Geophys. Res. Lett.*, *43*, 7982–7990, doi:10.1002/2016GL070083.

Received 30 JUN 2016
Accepted 24 JUL 2016
Accepted article online 29 JUL 2016
Published online 14 AUG 2016

Finite-frequency wave propagation through outer rise fault zones and seismic measurements of upper mantle hydration

Nathaniel C. Miller[1] and Daniel Lizarralde[2]

[1]U.S. Geological Survey, Woods Hole Science Center, Woods Hole, Massachusetts, USA, [2]Department of Geology and Geophysics, Woods Hole Oceanographic Institution, Woods Hole, Massachusetts, USA

Abstract Effects of serpentine-filled fault zones on seismic wave propagation in the upper mantle at the outer rise of subduction zones are evaluated using acoustic wave propagation models. Modeled wave speeds depend on azimuth, with slowest speeds in the fault-normal direction. Propagation is fastest along faults, but, for fault widths on the order of the seismic wavelength, apparent wave speeds in this direction depend on frequency. For the 5–12 Hz Pn arrivals used in tomographic studies, joint-parallel wavefronts are slowed by joints. This delay can account for the slowing seen in tomographic images of the outer rise upper mantle. At the Middle America Trench, confining serpentine to fault zones, as opposed to a uniform distribution, reduces estimates of bulk upper mantle hydration from ~3.5 wt % to as low as 0.33 wt % H_2O.

1. Introduction

Water has significant effects on the rheology and geochemistry of mantle rocks and plays a fundamental role in many geodynamic and geochemical processes on Earth [e.g., *Peacock*, 1990; *Hirth and Kohlstedt*, 2003; *Katz and Spiegelman*, 2003; *Faccenda*, 2014]. Water carried to depth by subducting oceanic lithosphere is the primary source of mantle rehydration, with the largest component potentially coming from the upper mantle [*Rupke*, 2004; *Hacker*, 2008; *van Keken et al.*, 2011]. The oceanic upper mantle is likely dehydrated by melt production at mid-ocean ridges [*Hirth and Kohlstedt*, 1996], but many recent studies argue that seawater moving along bending-induced faults at the outer rise provides a mechanism for rehydration just prior to subduction [e.g., *Ranero et al.*, 2003; *Faccenda et al.*, 2009; *Van Avendonk et al.*, 2011; *Shillington et al.*, 2015].

Seismic-reflection images appear to show that outer rise faults can extend into the uppermost mantle [*Ranero et al.*, 2003]. Numerical models support the existence of deep-cutting faults and suggest that negative pressure gradients created by plate bending can pump seawater into the upper mantle along these potential fluid pathways [*Faccenda et al.*, 2009]. If seawater does reach the upper mantle via bending faults, it would fill thin cracks with free water, react strongly with mantle peridotite to fill cracks and fault zones with serpentinite, and/or diffuse between fault zones, pervasively serpentinizing the upper mantle [e.g., *Faccenda*, 2014]. The particular distribution of a given volume of water in the upper mantle, as free water and serpentine minerals distributed diffusely and/or in cracks and/or fault zones, affects seismic wave speeds and thus wave speed-based estimates of water volume.

Estimates of the degree of serpentinization and water volume in the subducting upper mantle have come largely from tomographic images that show ~5 to 10% reductions in compressional wave speeds over the upper ~1 to 10 km of the mantle [e.g., *Walther et al.*, 2000; *Ranero and Sallares*, 2004; *Grevemeyer et al.*, 2007; *Ivandic et al.*, 2008, 2010; *Van Avendonk et al.*, 2011; *Lefeldt et al.*, 2012; *Fujie et al.*, 2013; *Shillington et al.*, 2015]. Mean seismic velocities in serpentinized rocks are slower than in unaltered rocks [*Christensen*, 1966; *Carlson and Miller*, 2003], and seismic velocity measurements have been used to infer degree of serpentinization using empirical relationships for uniformly distributed serpentine in isotropic media. For example, *Van Avendonk et al.* [2011] infer that the subducting upper mantle offshore Nicaragua is up to ~30% serpentinized and contains ~3.5 wt % H_2O, based on comparing measured velocities of ~6.7 to 7.6 km/s to a ~8.2 km/s mean (isotropic) wave speed for unaltered peridotites and assuming that serpentinization is uniformly distributed.

Fault zone geometry is likely to also affect wave speeds. Outer rise faults form by reactivation of abyssal hills during plate bending, or by breaking new faults in the bending-normal direction if the bending direction is

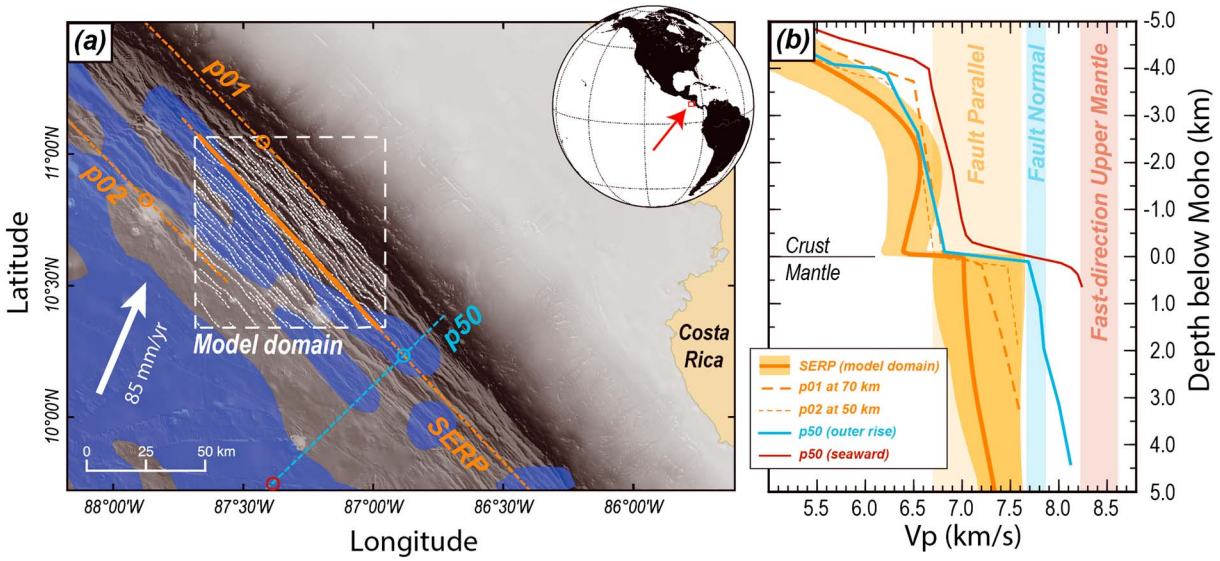

Figure 1. (a) Middle America Trench offshore Nicaragua and Costa Rica. Lines mark tomographic models: p50 [*Ivandic et al.*, 2008], p01/p02 [*Ivandic et al.*, 2010], and SERP [*Van Avendonk et al.*, 2011]. Negative magnetic anomalies on the incoming plate are shown in blue [*Maus et al.*, 2009]. White vector indicates relative Cocos/Caribbean plate motion [*Syracuse and Abers*, 2006]. (b) Velocity profiles from the outer rise in the three tomography lines shown in Figure 1a. For Lines p01, p02, and p50, profiles are from the locations marked by open circles in Figure 1a. For Line SERP, the shaded orange region indicates the range of velocities over the model domain in Figure 1a. Colored vertical bands mark the range of velocities over the upper 2 km of the mantle.

more than ~25° from the relic spreading direction [*Masson*, 1991]. In either case, the faults are generally parallel, and alignment of thin cracks and/or damage and serpentinization within fault zones (i.e., "joints") would create an extrinsic anisotropy. Effective media theory has been derived for uniform distributions of aligned cracks and joints that are much thinner than the seismic wavelength (e.g., ≪800 m for a 10 Hz upper mantle refraction at 8 km/s). For this thin crack/joint case, paths traveling in the fault-parallel direction have an effective wave speed that approaches that of the background material, with fault-perpendicular wave speeds changing as a function of crack aspect ratio/joint width and azimuth [*Crampin*, 1981; *Hudson*, 1981; *Thomsen*, 1995]. Thus, if cracks or joints are thin enough, traveltimes may be used to estimate pervasive serpentinization in the background mantle, as long as this anisotropy is accounted for.

Thin cracks/joints within a pervasively serpentinized mantle are, however, an unlikely scenario: If water does reach the upper mantle by downward pumping, faulting itself reduces pressure within the fault zone, promoting localization of fluids [*Faccenda et al.*, 2008; *Mancktelow*, 2008] and inhibiting diffusion of water into the surrounding mantle. Even if lateral pressure gradients decrease at depth (e.g., as bending faults approach the neutral plane in the plate), porosity may be quickly consumed by the large volume expansion (~50%) of serpentinization, limiting the access of water to unaltered mineral surfaces [*Klein et al.*, 2015] and restricting hydration to areas of active faulting.

Here we consider the alternative case where serpentinization is confined to joints that are wide with respect to the seismic wavelength. We use a numerical code to simulate wave propagation through the fault geometry observed on the seafloor at the outer rise of the Middle America Trench (MAT) (Figure 1). The numerical approach is able to test the effect of fault width and geometry on finite-frequency wave propagation, which cannot be handled by existing analytic solutions for wave speed in uniformly cracked or jointed media [e.g., *Hudson*, 1981]. The upper mantle under the outer rise of the MAT has been imaged along fault-parallel and fault-normal directions by wide-angle seismic experiments [*Walther et al.*, 2000; *Ivandic et al.*, 2008; *Van Avendonk et al.*, 2011]. We compare the modeling results to those observations and discuss implications for finite-frequency, seismic-based estimates of upper mantle hydration.

2. Methods

We modeled wide joints in the upper mantle as low-velocity zones embedded in a faster background material. The models are 2-D and represent a horizontal slice through the mantle, analogous to transversely

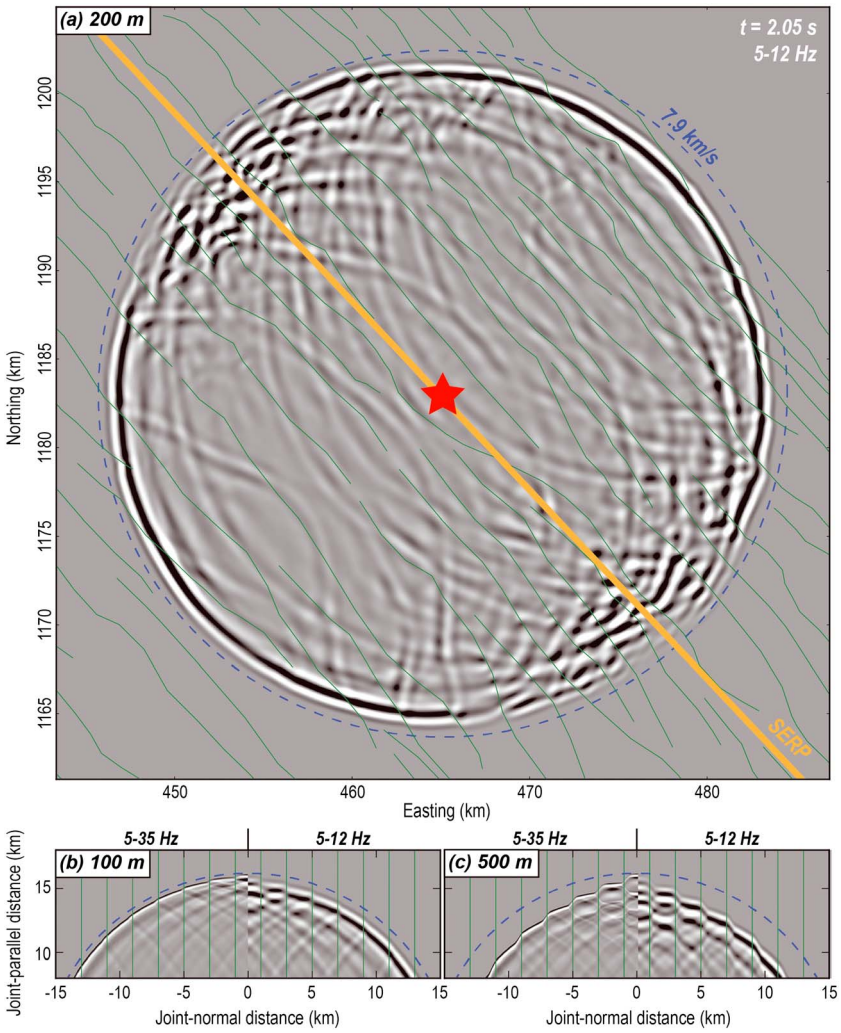

Figure 2. (a) Wavefield at 2.05 s for a 5–12 Hz point source (star) propagating through a realistic geometry of 200 m wide, 5 km/s serpentinite joints (green lines) in a 7.9 km/s background mantle. The orange line marks the position of Line SERP [*Van Avendonk et al*., 2011] relative to the surface fault traces observed at the MAT. Coordinates are Universal Transverse Mercator Zone 16 North. (b and c) Comparison of wavefields at 2.05 s for 5–35 (left) and 5–12 Hz (right) sources propagating through 100 (Figure 2b) and 500 m (Figure 2c) wide, parallel joints. In all, the dashed blue line shows the position of a wavefront traveling at the background mantle wave speed of 7.9 km/s.

isotropic media in long-wavelength analytic solutions for vertically aligned cracks or joints [e.g., *Hudson*, 1981]. We considered two fault geometries: (1) regularly spaced, parallel faults (Figures 2b and 2c) and (2) a realistic fault geometry (Figure 2a) based on fault offsets observed in bathymetric data [*Weinrebe and Ranero*, 2012] over a ~100 by 100 km region on the outer rise offshore Nicaragua (Figure 1), where major bending-related faults are spaced every ~2 km. Bending faults may extend up to ~8 km into the mantle [*Ranero et al*., 2003], and we assume that joints in the upper mantle would have a similar geometry as the faults observed on the seafloor. We tested the effect of joint width on wave propagation by running models with 100, 200, and 500 m wide low-velocity zones. These widths are similar to the width of conductive anomalies attributed to high-porosity fault zones in the crust [*Naif et al*., 2015], as well as the width of localized upper mantle hydration in numerical models [e.g., *Faccenda et al*., 2008]. To resolve these low-velocity zones, we required that there be at least four grid points per joint width and used a grid spacing of 25 m in both directions for all models.

We assumed that the model joints are 100% serpentinized and assigned the fault-zone material a velocity of 5.0 km/s, consistent with mean wave speeds measured in chrysotile- and lizardite-bearing serpentinites [*Christensen*, 1966; *Carlson and Miller*, 2003]. Corner flow at mid-ocean ridges creates a crystal-preferred

orientation of intrinsically anisotropic minerals in the upper mantle [*Zhang and Karato*, 1995; *Jung and Karato*, 2001], causing the bulk upper mantle to be anisotropic with a fast direction oriented in the spreading direction and slow wave speeds in the spreading-perpendicular direction [*Ismaıl and Mainprice*, 1998; *Kaminski and Ribe*, 2001, 2002]. The model region is centered on *Van Avendonk et al.'s* [2011] Line SERP, which is perpendicular to the relic spreading direction, as inferred from magnetic anomalies (Figure 1), and thus in the slow direction for the incoming mantle fabric. To compare the model results directly to the Line SERP tomography, we assigned the background mantle a constant velocity of 7.9 km/s, approximately the slow-direction wave speed measured in the Pacific upper mantle [*Kawasaki and Kon'no*, 1984; *Shearer and Orcutt*, 1986].

We modeled wave propagation through the joint models using a 2-D pseudospectral acoustic code based on *Kosloff and Baysal* [1982]. The method solves the acoustic wave equation by calculating spatial derivatives in the wave number domain and time derivatives by second-order differences. A source wavelet was introduced at the center of the model domain at time zero. We defined this source as the response of a minimum-phase Butterworth filter with corner frequencies between 5 and 35 Hz, which produces wavelengths of 143 to 1580 m for the 5.0 to 7.9 km/s model velocities. The pseudospectral method is accurate for grid spacings as large as two points per wavelength [*Kosloff and Baysal*, 1982], or 72 m at 35 Hz and 5.0 km/s, which is above the 25 m grid spacing needed to resolve the joint widths.

We tested the effect of frequency on wave speeds by propagating 5 to 35 Hz and 5 to 12 Hz sources through all models. We picked first arrival traveltimes on unfiltered waveforms using an automated method based on the ratio of root-mean-square amplitude for short versus long sliding time windows, a common approach for automatic picking in real data.

3. Results and Discussion

We modeled acoustic-wave propagation though 100, 200, and 500 m wide, serpentinized joints in a uniform, background mantle. Effective wave speeds in these models are anisotropic, with slower wave speeds in the joint-perpendicular direction and faster wave speeds parallel to joints, with wavefronts in the background media overtaking slower guided waves within joints (Figure 2). This anisotropy is qualitatively similar to effective-media theory for thin joints (i.e., long wavelengths) [e.g., *Hudson*, 1981]. That theory also predicts fastest wave speeds in the joint-parallel direction with slowest wave speeds in the joint-normal direction, but it is not valid in the wide-joint (short wavelength) case that we modeled.

The traveltime of a finite-frequency wavefront is sensitive to wave speeds over a finite width that is proportional to wavelength, rather than along infinitesimally thin raypaths. The upper mantle refraction phase (i.e., "Pn") used in tomography is typically strongest at ~5 to 12 Hz [e.g., *Van Avendonk et al.*, 2011]. For a constant wave speed of ~8 km/s, finite-frequency Fréchet sensitivity kernels [e.g., *Spetzler and Snieder*, 2004] for this band are up to ~10 km wide [*Collins and Molnar*, 2014]. This width is greater than the typical ~2 km spacing of bending-related faults (Figure 1), suggesting that even waves traveling in the fast, joint-parallel direction would be slowed by low-velocity joints.

The band-limited wavefronts in the acoustic models are dispersive. For a ~35 Hz phase, joint-parallel traveltimes approach those of the background mantle in all models (Figures 3a–3c). In contrast, the strongest arrival from the 5 to 12 Hz Pn band is slower than the background mantle in even the fast direction (Figures 3d–3f). This delay increases with increasing joint width, as the proportion of slower, joint-filling material increases. Dispersion is most clearly observed in models with exactly parallel joints (Figures 2b and 2c), since fault-parallel paths never cross joints in this simplified geometry.

The acoustic models demonstrate how chaotic the seismic wavefront can become as it propagates through outer rise faults, even for simple models that lack, for example, scattering by crustal structure or a heterogenous background mantle. The synthetic data also benefit from an unrealistically dense receiver spacing, which improves trace-to-trace coherency and makes identifying arrivals much easier than in actual experiment geometries. The wavefront is most disrupted by faults in fault-parallel directions, making first arrivals in this direction difficult to distinguish from the larger-amplitude, later-arriving guided waves (Figures 3g–3i). Line SERP was acquired along this fault-parallel azimuth, and scattering from faults likely accounts, at least partly, for the poor data quality reported by *Van Avendonk et al.* [2011].

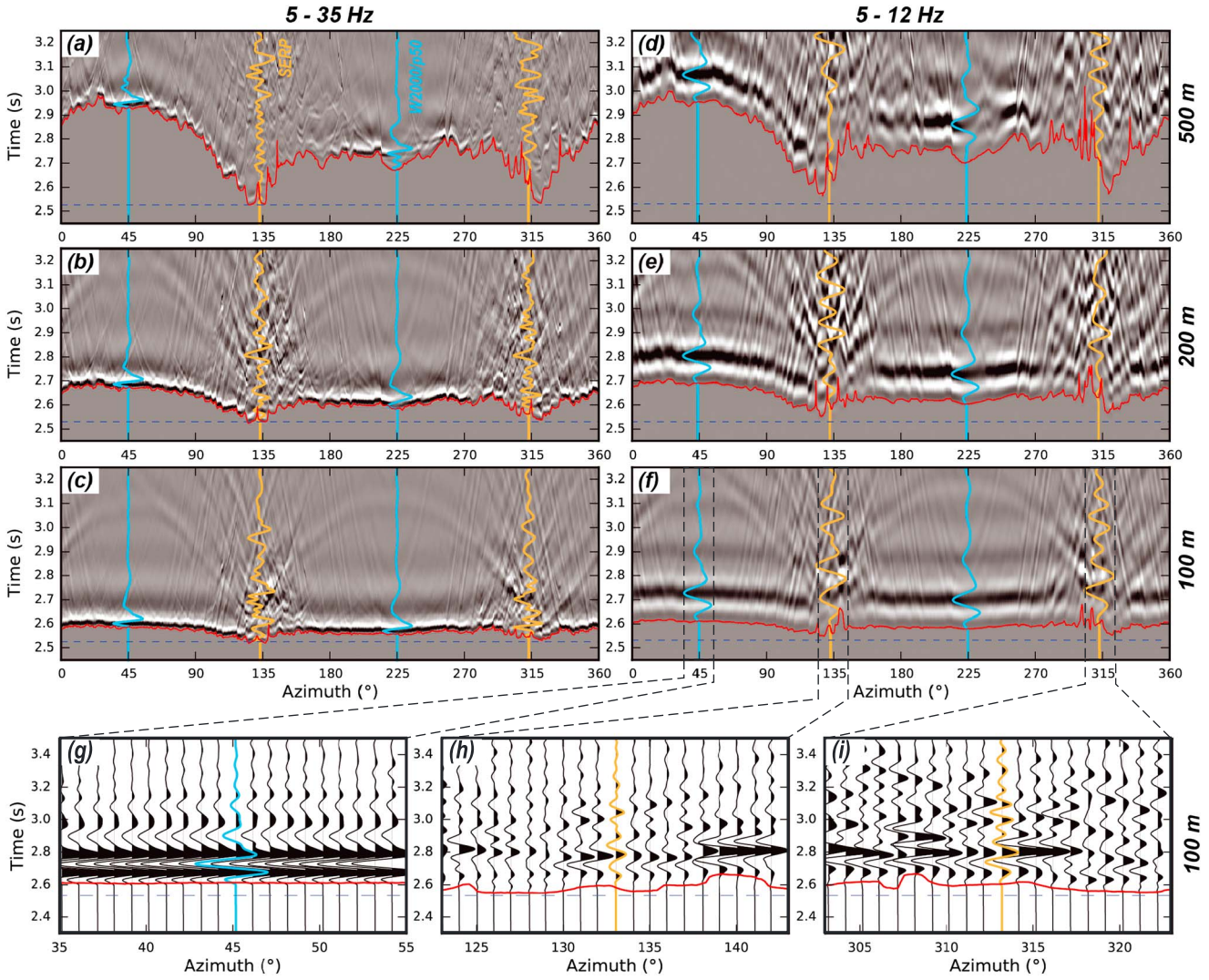

Figure 3. Amplitude as a function of time and azimuth at 20 km offset for models with 500, 200, and 100 m wide serpentinized joints. Source wavelet is the response of a minimum-phase Butterworth filter with corner frequencies at (a–c) 5 and 35 Hz and (d–f) 5 and 12 Hz. (g–i) Wiggle plot details from Figure 3f. Red lines mark picks made using a short/long windowed amplitude ratio. The dashed line marks the traveltime of a wavefront traveling at the background mantle velocity of 7.9 km/s, and vertical lines mark tomography lines in Figure 1.

Anisotropy from joints at the outer rise will overprint preexisting anisotropy in the incoming upper mantle, and interpretations of upper mantle wave speeds should account for both relic fabric and joints. The Cocos Plate subducting offshore Nicaragua was produced at the East Pacific Rise [e.g., *Barckhausen et al.*, 2001], and likely has a similar upper mantle fabric as the Pacific Plate. The Pacific is ~7% anisotropic, with a ~8.4 to 8.6 km/s fast direction oriented in the relic spreading direction and a ~7.9 to 8.0 km/s slow, spreading-normal direction [e.g., *Kawasaki and Kon'no*, 1984; *Shearer and Orcutt*, 1986]. Magnetic anomalies at the outer rise of the MAT indicate that the relic spreading direction, and therefore the relic fast direction, is oriented approximately perpendicular to the bending-related faults (Figure 1a), which is the slow direction in the joint models. Line p50 is oriented along the inferred relic fast direction and indicates that the incoming, unaltered upper-most mantle is ~8.2 km/s in the fast direction (Figure 1b).

A combination of inherited upper mantle anisotropy and modeled delay times at Pn frequencies from 100 to 500 m wide joints can explain nearly all the slowing observed in tomographic images of the subducting upper mantle at the MAT (Figure 4). In the region we modeled, Line SERP images velocities over the upper 2 km of the mantle of ~6.7 to 7.6 km/s (orange band in Figure 4). Line SERP is oriented perpendicular to the relic spreading direction, and the incoming mantle is already slow (~7.9 to 8.0 km/s) in this direction.

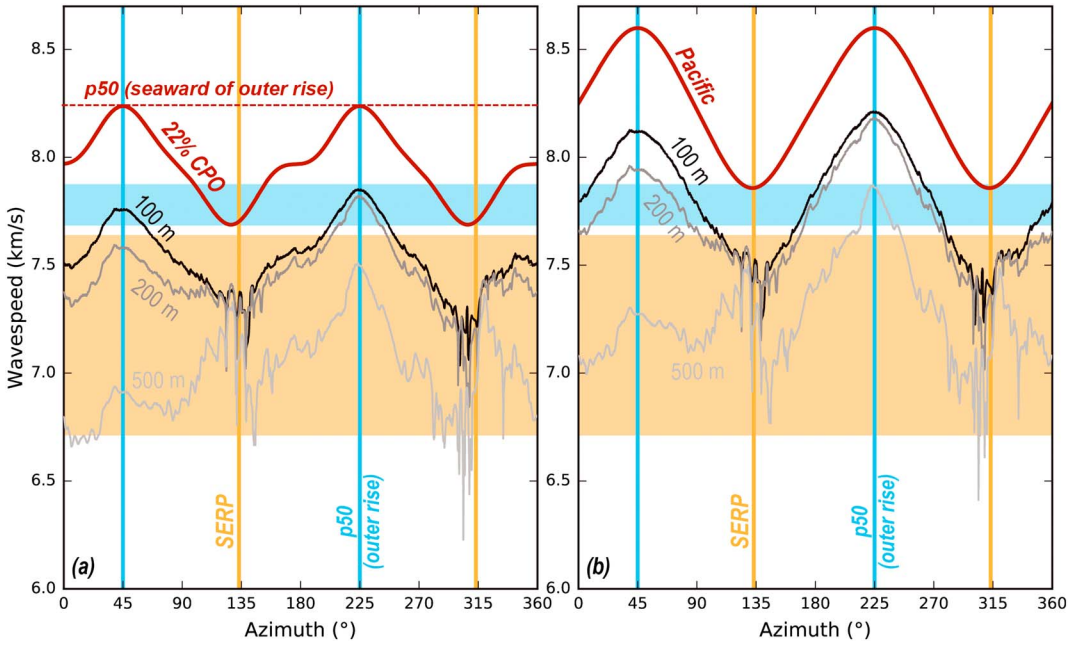

Figure 4. Wave speed as a function of azimuth for an unaltered upper mantle (thick red lines) slowed by 100, 200, and 500 m wide serpentinite joints (thin black to gray lines). (a) Unaltered mantle wave speeds are calculated by shifting fast-direction wave speeds in a model of 22% alignment of upper mantle olivine grains [*Shearer and Orcutt*, 1986] to match the ~8.2 km/s upper mantle velocity observed seaward of the outer rise along Line p50 [*Ivandic et al.*, 2008]. (b) Unaltered mantle wave speeds are from the Pacific upper mantle measurements of *Kawasaki and Kon'no* [1984]. Colored, horizontal bands show the range of upper mantle velocities from tomography models for Lines p50 (blue) and SERP (orange) [*Van Avendonk et al.*, 2011]. Vertical lines mark azimuths of the tomography models in Figure 1.

The acoustic models indicate that the presence of 100 to 500 m wide joints would slow the upper mantle by an additional ~0.5 to 0.8 km/s, giving absolute, slow-direction wave speeds of ~6.9 to 7.4 km/s—similar to the Line SERP velocities (Figure 4). Line p50 [*Ivandic et al.*, 2008] is oriented in the fault-normal direction, perpendicular to Line SERP. At the outer rise, uppermost mantle velocities are ~7.7 to 7.9 km/s along this orientation, faster than the fault-parallel Line SERP and consistent with the composite relic mantle plus joint models (Figure 4).

Comparisons of absolute wave speeds in Figure 4 depend on the choice of a reference model for the incoming upper mantle, as well as the model geometry and velocities from tomographic models. We calculated wave speed curves for joints in a relic mantle using two models for inherited upper mantle anisotropy: (1) a model in which anisotropy from 22% alignment of olivine grains is shifted such that the fast direction matches prefaulting, fast-direction velocities on Line p50 (Figure 4a) and (2) an anisotropy model for the Pacific upper mantle based on observed traveltimes in active source data [*Kawasaki and Kon'no*, 1984] (Figure 4b). Uncertainty in the reference models likely exceeds the ±0.05 to ±0.1 km/s uncertainty reported for the tomographic models [*Ivandic et al.*, 2008; *Van Avendonk et al.*, 2011]. Of the tested models, a combination of the reference model based on 22% alignment of olivine grains and Line p50 with 100 m wide joints produces the best fit to observations, but either reference model can produce wave speeds that are generally consistent with the tomographic models.

The acoustic models show that far less serpentine is needed to achieve a given traveltime delay if the serpentine is confined to joints rather than distributed uniformly. This result has significant implications for estimates of the water input to subduction zones. The weight fraction of water (w_h) bound in a partially serpentinized peridotite can be estimated as follows [*Carlson and Miller*, 2003]:

$$w_h = \frac{w_s \alpha_s \rho_s}{(1-\alpha_s)\rho_m + \alpha_s \rho_s} \quad (1)$$

where $w_s \approx 0.13$ is the weight fraction of water in serpentine, α_s is the volume fraction of serpentine, $\rho_s \approx 2485\ \mathrm{kg/m^3}$ is the density of serpentine, and $\rho_m \approx 3400\ \mathrm{kg/m^3}$ is the density of unaltered peridotite. If

the upper mantle is uniformly serpentinized, Line SERP velocities suggest that the upper mantle is ~30% serpentinized, which, based on equation (1), contains ~3.5 wt % H_2O [*Van Avendonk et al*., 2011]. In contrast, 100% serpentinization of 500 m wide joints gives a bulk serpentinization volume of ~17%, or ~1.7 wt % H_2O, when serpentine-bound water localized within fault zones with the geometry observed offshore Nicaragua is averaged over the total model area. Similarly, 200 and 100 m wide joints would give ~6.8 and 3.4% serpentine by total volume, or ~0.66 and ~0.33 wt % H_2O.

Wet cracks, rather than serpentinized peridotite, could also produce slow velocity, joint-filling material, but with even less water. Adding just 1% randomly oriented, crack-like porosity to mantle rocks can reduce compressional wave speeds by 20% with just ~0.3 wt % water [*Korenaga et al*., 2002; J. Korenaga, personal communication, 2015]—more than an order of magnitude less than the ~3.5 wt % water contained in the 30% serpentinization needed to achieve the same slowing. Restricting crack porosity to wide fault zones would have a similar effect on wave speeds as the modeled low-velocity joints, but, for 500 m wide joints offshore Nicaragua, would require only 17% cracked material by volume and have a bulk water content of just ~0.05 wt % to explain the field observations.

The crack-only, no-serpentine case is a minimal-water, end-member model. Seawater in contact with upper mantle peridotite reacts to produce serpentine [*Ulmer and Trommsdorff*, 1995; *Klein et al*., 2015]. Although it is unclear how efficient serpentinization is at upper mantle pressures (Korenaga, personal communication, 2015), the acoustic models show that the presence of at least some degree of serpentinization cannot be excluded by the tomographic observations. Even if alteration extends hundreds of meters from fault zones, much less water is needed to explain observed velocities than models of pervasive serpentinization.

Finally, the modeling results highlight the importance of experiment design when measuring seismic properties in a wide-joint setting. The results demonstrate that effective azimuthal wave speed variation is a function of experiment geometry (i.e., source and receiver locations) and fault geometry, which together determine the number of joints crossed along a particular raypath. An example of this dependence is the wavefront asymmetry between azimuths 0° to 180° versus 180° to 360° seen in Figure 3. The shape of this delay-time curve is due to the fault geometry at the MAT, and this shape would be different for a different fault geometry and/or experiment geometry. Source/receiver offset also has an effect on observed delay time from joints, because of both the relationship between offset and number and joints crossed and accrual of finite-frequency effects with propagation distance. In the models, we measured traveltimes and effective wave speeds for a mantle propagation distance of 20 km (corresponding to 35–40 km offset from a sea surface to a seafloor receiver). Pn paths that sample the uppermost mantle in the tomographic models turn immediately below the Moho or propagate along nearly horizontal paths for up to ~35 km [*Van Avendonk et al*., 2011], and velocity at any one point in the tomographic models is constrained by raypaths with a range of mantle propagation distances and thus joint crossings. Finite-frequency sensitivity also scales with distance, compounding the effect of source-receiver offset on delay time observations. In active-source experiments, wavefronts disperse while propagating through the water column and crust before and after traveling through the mantle, causing wavefields to be sensitive to velocities over a wider region than in the models. Since changing the particular combination of source-receiver layout and fault geometry has a similar effect as changing the amount of joint material along a raypath, effects on apparent wave speeds are likely similar in magnitude to the asymmetry and differences between models with different fault widths seen in Figure 4. These models differ by up to ~0.9 km/s, and these effects must be considered in observational studies.

4. Conclusions

We modeled wave propagation through low-velocity joints in a background, uniform mantle in order to assess the azimuthal dependence of wave speed and wavefront characteristics in a realistically jointed media. We considered joint widths of 100, 200, and 500 m, which are on the order of the wavelength of upper mantle refraction phase Pn. Traveltimes through these models are anisotropic, with slowest speeds in the joint-normal direction. Propagation is fastest along the joints, but apparent wave speeds in this direction depend on frequency. For the 5–12 Hz band Pn arrivals used in tomographic studies, joint-parallel wavefronts are slowed by joints.

Slowing from joints, along with anisotropy inherited from the incoming upper mantle, can account for the observed slowing in the upper mantle under the outer rise of the MAT. Explaining the observed slowing with

serpentinization confined to joints, rather than via pervasive serpentinization, reduces estimates of bulk serpentinization from up to ~30% to as low as ~3.4% by volume and reduces corresponding estimates of bulk upper mantle water content from ~3.5 wt % to as low as 0.33 wt %.

This modeling exercise highlights problems of nonuniqueness in seismic estimates of outer rise hydration. Nonetheless, the model of serpentinized (or cracked) fault zones considered here can reconcile slow seismic velocities observed at the outer rise, both offshore Nicaragua and at many other subduction zones, with the theoretical prediction that fluids and serpentinization would localize along fault zones.

Acknowledgments
Synthetic data are available from N.M. This work was supported by NSF grant OCE-0841063 to D.L. This manuscript benefited from thoughtful discussions with John Collins; reviews by Jun Korenaga and access to his paper in review on cracking and mantle hydration during plate bending; and input from an anonymous reviewer. Maps and figures were plotted with QGIS [*QGIS Development Team*, 2015] and matplotlib [*Hunter*, 2007].

References

Barckhausen, U., C. R. Ranero, R. Von Huene, S. C. Cande, and H. A. Roeser (2001), Revised tectonic boundaries in the Cocos Plate off Costa Rica: Implications for the segmentation of the convergent margin and for plate tectonic models, *J. Geophys. Res.*, *106*(B9), 19,207–19,220, doi:10.1029/2001JB000238.

Carlson, R. L., and D. J. Miller (2003), Mantle wedge water contents estimated from seismic velocities in partially serpentinized peridotites, *Geophys. Res. Lett.*, *30*(5), 1250, doi:10.1029/2002GL016600.

Christensen, N. I. (1966), Elasticity of ultrabasic rocks, *J. Geophys. Res.*, *71*(24), 5921–5931, doi:10.1029/JZ071i024p05921.

Collins, J. A., and P. Molnar (2014), Pn anisotropy beneath the South Island of New Zealand and implications for distributed deformation in continental lithosphere, *J. Geophys. Res. Solid Earth*, *119*, 7745–7767, doi:10.1002/2014JB011233.

Crampin, S. (1981), A review of wave motion in anisotropic and cracked elastic-media, *Wave Motion*, *3*(4), 343–391.

Faccenda, M. (2014), Water in the slab: A trilogy, *Tectonophysics*, doi:10.1016/j.tecto.2013.12.020.

Faccenda, M., L. Burlini, T. V. Gerya, and D. Mainprice (2008), Fault-induced seismic anisotropy by hydration in subducting oceanic plates, *Nature*, *455*(7216), 1097–1100, doi:10.1038/nature07376.

Faccenda, M., T. V. Gerya, and L. Burlini (2009), Deep slab hydration induced by bending-related variations in tectonic pressure, *Nat. Geosci.*, doi:10.1038/ngeo656.

Fujie, G., S. Kodaira, M. Yamashita, and T. Sato (2013), Systematic changes in the incoming plate structure at the Kuril trench, *Geophys. Res. Lett.*, *40*, 88–93, doi:10.1029/2012GL054340.

Grevemeyer, I., C. R. Ranero, E. R. Flueh, D. Kläschen, and J. Bialas (2007), Passive and active seismological study of bending-related faulting and mantle serpentinization at the Middle America trench, *Earth Planet. Sci. Lett.*, *258*(3–4), 528–542, doi:10.1016/j.epsl.2007.04.013.

Hacker, B. R. (2008), H_2O subduction beyond arcs, *Geochem. Geophys. Geosyst.*, *9*, Q03001, doi:10.1029/2007GC001707.

Hirth, G., and D. Kohlstedt (2003), Rheology of the upper mantle and the mantle wedge: A view from the experimentalists, in *Inside the Subduction Factory*, vol. 138, pp. 83–105, AGU, Washington, D. C.

Hirth, G., and D. L. Kohlstedt (1996), Water in the oceanic upper mantle: Implications for rheology, melt extraction and the evolution of the lithosphere, *Earth Planet. Sci. Lett.*, *144*(1–2), 93–108, doi:10.1016/0012-821X(96)00154-9.

Hudson, J. A. (1981), Wave speeds and attenuation of elastic waves in material containing cracks, *Geophys. J. R. Astron. Soc.*, *64*(1), 133–150, doi:10.1111/j.1365-246X.1981.tb02662.x.

Hunter, J. D. (2007), Matplotlib: A 2D graphics environment, *Comput. Sci. Eng.*, *9*(3), 90–95.

Ismaıl, W. B., and D. Mainprice (1998), An olivine fabric database: An overview of upper mantle fabrics and seismic anisotropy, *Tectonophysics*, *296*(1), 145–157.

Ivandic, M., I. Grevemeyer, A. Berhorst, E. R. Flueh, and K. McIntosh (2008), Impact of bending related faulting on the seismic properties of the incoming oceanic plate offshore of Nicaragua, *J. Geophys. Res.*, *113*, B05410, doi:10.1029/2007JB005291.

Ivandic, M., I. Grevemeyer, J. Bialas, and C. J. Petersen (2010), Serpentinization in the trench-outer rise region offshore of Nicaragua: Constraints from seismic refraction and wide-angle data, *Geophys. J. Int.*, *180*(3), 1253–1264.

Jung, H., and S. Karato (2001), Water-induced fabric transitions in olivine, *Science*, *293*(5534), 1460–1463.

Kaminski, E., and N. M. Ribe (2001), A kinematic model for recrystallization and texture development in olivine polycrystals, *Earth Planet. Sci. Lett.*, *189*(3–4), 253–267, doi:10.1016/S0012-821X(01)00356-9.

Kaminski, É., and N. M. Ribe (2002), Timescales for the evolution of seismic anisotropy in mantle flow, *Geochem. Geophys. Geosyst.*, *3*(8), 1051, doi:10.1029/2001GC000222.

Katz, R. F., and M. Spiegelman (2003), A new parameterization of hydrous mantle melting, *Geochem. Geophys. Geosyst.*, *4*(9), 1073, doi:10.1029/2002GC000433.

Kawasaki, I., and F. Kon'no (1984), Azimuthal anisotropy of surface waves and the possible type of the seismic anisotropy due to preferred orientation of olivine in the uppermost mantle beneath the Pacific Ocean, *J. Phys. Earth*, *32*(3), 229–244.

Klein, F., N. G. Grozeva, J. S. Seewald, T. M. McCollom, S. E. Humphris, B. Moskowitz, T. S. Berquo, and W. A. Kahl (2015), Experimental constraints on fluid-rock reactions during incipient serpentinization of harzburgite, *Am. Mineral.*, *100*(4), 991–1002.

Korenaga, J., P. B. Kelemen, and W. S. Holbrook (2002), Methods for resolving the origin of large igneous provinces from crustal seismology, *J. Geophys. Res.*, *107*(B9), 2178, doi:10.1029/2001JB001030.

Kosloff, D. D., and E. Baysal (1982), Forward modeling by a Fourier method, *Geophysics*, *47*(10), 1402–1412.

Lefeldt, M., C. R. Ranero, and I. Grevemeyer (2012), Seismic evidence of tectonic control on the depth of water influx into incoming oceanic plates at subduction trenches, *Geochem. Geophys. Geosyst.*, *13*, Q05013, doi:10.1029/2012GC004043.

Mancktelow, N. S. (2008), Tectonic pressure: Theoretical concepts and modelled examples, *Lithos*, *103*(1–2), 149–177, doi:10.1016/j.lithos.2007.09.013.

Masson, D. G. (1991), Fault patterns at outer trench walls, *Mar. Geophys. Res.*, *13*(3), 209–225.

Maus, S., et al. (2009), EMAG2: A 2–arc min resolution Earth Magnetic Anomaly Grid compiled from satellite, airborne, and marine magnetic measurements, *Geochem. Geophys. Geosyst.*, *10*, Q08005, doi:10.1029/2009GC002471.

Naif, S., K. Key, S. Constable, and R. L. Evans (2015), Water-rich bending faults at the Middle America Trench, *Geochem. Geophys. Geosyst.*, *16*, 2582–2597, doi:10.1002/2015GC005927.

Peacock, S. A. (1990), Fluid processes in subduction zones, *Science*, *248*(4953), 329–337, doi:10.1126/science.248.4953.329.

QGIS Development Team (2015), QGIS Geographic Information System, *Open Source Geospatial Foundation Project*.

Ranero, C. R., and V. Sallares (2004), Geophysical evidence for hydration of the crust and mantle of the Nazca plate during bending at the north Chile trench, *Geology*, *32*(7), 549–552, doi:10.1130/G20379.1.

Ranero, C. R., J. P. Morgan, K. McIntosh, and C. Reichert (2003), Bending-related faulting and mantle serpentinization at the Middle America trench, *Nature*, *425*(6956), 367–373.

Rupke, L. (2004), Serpentine and the subduction zone water cycle, *Earth Planet. Sci. Lett.*, *223*(1–2), 17–34, doi:10.1016/j.epsl.2004.04.018.

Shearer, P. M., and J. A. Orcutt (1986), Compressional and shear wave anisotropy in the oceanic lithosphere—The Ngendei seismic refraction experiment, *Geophys. J. Int.*, *87*(3), 967–1003, doi:10.1111/j.1365-246X.1986.tb01979.x.

Shillington, D. J., A. Bécel, M. R. Nedimović, H. Kuehn, S. C. Webb, G. A. Abers, K. M. Keranen, J. Li, M. Delescluse, and G. A. Mattei-Salicrup (2015), Link between plate fabric, hydration and subduction zone seismicity in Alaska, *Nat. Geosci.*, *8*(12), 961–964, doi:10.1038/ngeo2586.

Spetzler, J., and R. Snieder (2004), The Fresnel volume and transmitted waves, *Geophysics*, *69*(3), 653–663, doi:10.1190/1.1759451.

Syracuse, E. M., and G. A. Abers (2006), Global compilation of variations in slab depth beneath arc volcanoes and implications, *Geochem. Geophys. Geosyst.*, *7*, Q05017, doi:10.1029/2005GC001045.

Thomsen, L. (1995), Elastic anisotropy due to aligned cracks in porous rock, *Geophys. Prospect.*, *43*(6), 805–829, doi:10.1111/j.1365-2478.1995.tb00282.x.

Ulmer, P., and V. Trommsdorff (1995), Serpentine stability to mantle depths and subduction-related magmatism, *Science*, *268*(5212), 858–861.

Van Avendonk, H. J. A., W. S. Holbrook, D. Lizarralde, and P. Denyer (2011), Structure and serpentinization of the subducting Cocos plate offshore Nicaragua and Costa Rica, *Geochem. Geophys. Geosyst.*, *12*, Q06009, doi:10.1029/2011GC003592.

van Keken, P. E., B. R. Hacker, E. M. Syracuse, and G. A. Abers (2011), Subduction factory: 4. Depth-dependent flux of H_2O from subducting slabs worldwide, *J. Geophys. Res.*, *116*, B01401, doi:10.1029/2010JB007922.

Walther, C. H. E., E. R. Flueh, C. R. Ranero, R. Von Huene, and W. Strauch (2000), Crustal structure across the Pacific margin of Nicaragua: Evidence for ophiolitic basement and a shallow mantle sliver, *Geophys. J. Int.*, *141*(3), 759–777, doi:10.1046/j.1365-246x.2000.00134.x.

Weinrebe, W., and C. R. Ranero (2012), Multibeam bathymetry compilation of the Central America Pacific Margin, *Integr. Earth Data Appl.*, doi:10.1594/IEDA/100069.

Zhang, S., and S.-I. Karato (1995), Lattice preferred orientation of olivine aggregates deformed in simple shear, *Nature*, *375*(6534), 774–777.